frontiers in Earth Science

ORIGINAL RESEARCH
published: 24 January 2022
doi: 10.3389/feart.2022.694939

Crystal-Chemical and Structural Characterization of Omphacite in High-Pressure Eclogites From the Arquía Complex on Southwestern Pijao, Central Cordillera (Colombian Andes)

Oscar Mauricio Castellanos-Alarcón[1,2], *Karoll Michelle Cedeño Villarreal*[3], *Robert Antonio Toro Hernández*[3], *Carlos Alberto Ríos-Reyes*[4]*, *José Antonio Henao-Martínez*[3] and *Carlos Augusto Zuluaga-Castrillón*[2]

[1]Grupo de Investigación en Geofísica y Geología, Programa de Geología, Universidad de Pamplona, Villa del Rosario, Colombia, [2]Grupo de Investigación en Técnicas Aplicadas a Tectónica y Análisis de Cuencas, Departamento de Geociencias, Universidad Nacional de Colombia—Sede Bogotá, Bogotá, Colombia, [3]Grupo de Investigación en Química Estructural, Escuela de Química, Universidad Industrial de Santander, Bucaramanga, Colombia, [4]Grupo de Investigación en Geología Básica y Aplicada, Escuela de Geología, Universidad Industrial de Santander, Bucaramanga, Colombia

OPEN ACCESS

Edited by:
Fabrice Brunet,
Institut des Sciences de la Terre (ISTERRE), France

Reviewed by:
Fabrizio Nestola,
University of Padua, Italy
Shah Wali Faryad,
Charles University, Czechia

***Correspondence:**
Carlos Alberto Ríos-Reyes
carios@uis.edu.co

Specialty section:
This article was submitted to Earth and Planetary Materials, a section of the journal Frontiers in Earth Science

Received: 23 April 2021
Accepted: 04 January 2022
Published: 24 January 2022

Citation:
Castellanos-Alarcón OM, Cedeño Villarreal KM, Toro Hernández RA, Ríos-Reyes CA, Henao-Martínez JA and Zuluaga-Castrillón CA (2022) Crystal-Chemical and Structural Characterization of Omphacite in High-Pressure Eclogites From the Arquía Complex on Southwestern Pijao, Central Cordillera (Colombian Andes). Front. Earth Sci. 10:694939. doi: 10.3389/feart.2022.694939

Omphacite found in eclogites from the Arquía Complex (Colombia) was characterized using scanning electron microscopy, electron probe microanalysis and single-crystal X-ray diffraction. The sample is chemically homogeneous. Omphacite usually shows symplectitic intergrowths or a relictic character partially and totally included in amphibole. The transformation of omphacite to symplectites colonies characterizes the initiation of the eclogites retrograde metamorphism. The reaction history can be summarized as the decomposition of omphacite into symplectites as a product of decompression through the reaction: omphacite + quartz = plagioclase + clinopyroxene (low in Na), which can be considered as a discontinuous precipitation reaction. The structure of the studied omphacite single-crystal is successfully refined in the *P2/c* space group. This structure is interpreted as an intermediate towards omphacite with space group *P2/n*. The structure of omphacite shows silicate chains formed by two crystallographically different silicon tetrahedra (T1 and T2) with an O2-O3-O2 angle of 169.002 (2)°, indicating that the chain is slightly distorted. The Na and Ca cations occupy the octahedral and 8-coordination sites. Fe occurs as Fe^{2+} and Fe^{3+} and are distributed over the octahedral sites M1 and M11, respectively.

Keywords: eclogites, high-pressure, subduction slab, arquía complex, omphacite

INTRODUCTION

Eclogites are widely spread in metamorphic belts of high-pressure and/or ultrahigh-pressure worldwide (e.g., Miyagi and Takasu, 2005; Kabir and Takasu, 2010; Nakano et al., 2010; Li et al., 2016; Arrieta-Prieto et al., 2020; Xie et al., 2020; Feng et al., 2021; Schorn et al., 2021; Wang et al., 2021). They are important witnesses of subduction-collision processes (e.g., Sizova et al.,

2010; van Hunen and Moyen, 2012). Omphacite is a member of the clinopyroxene group of silicate minerals with the chemical formula (Ca,Na) (Mg,Fe,Al)[Si_2O_6]. It can contain Fe^{3+} and Fe^{2+} as acmite, $NaFe^{3+}Si_2O_6$, and hedenbergite, $CaFe^{2+}Si_2O_6$, respectively (e.g., Katerinopoulou et al., 2007). It represents a major constituent of eclogites, which play a key role in mantle convection and geodynamics in subduction zones. Omphacite provides valuable information on pressure–temperature conditions of high- to ultrahigh-pressure metamorphic rocks formed from basalts or gabbros in subduction zones (e.g., Nakamura and Banno, 1997; Zhang et al., 2006; Zhang and Green, 2007; Shu et al., 2014; Aulbach and Arndt, 2019). Omphacite can form in different environments where it can bring valuable thermobarometric constraints (e.g., Sheng and Gong, 2017; Ashchepkov et al., 2019; Liu et al., 2021). One of the main challenges for geologists investigating high-pressure rocks is to determine the mechanism and processes of exhumation. It is also clear that during exhumation, high-pressure rocks undergo, among other important processes, cooling, decompression and hydration of their main mineral phases, triggering retrogradation to amphibolite, epidote-amphibolite and green schist facies, with a notorious and easily differentiable symplectitic stage. Several authors discuss the occurrence of several stages of development of omphacite (e.g., Buatier et al., 1991; Su et al., 2011; Martin and Duchêne, 2015). Omphacite compositions are intermediate between calcium-rich augite and sodium-rich jadeite (Su et al., 2011). Previous investigations have already addressed the crystal chemistry of omphacites (e.g., Matsumoto et al., 1975; Rossi et al., 1983), its phase transitions (e.g., Carpenter, 1981; Pavese et al., 2000) and the solid solution properties along the augite—jadeite joint (Ballaran et al., 1998). In relation to subduction zone metamorphism, omphacite coexisting with jadeite or augite has attracted a great deal of attention for studies of the nature of sodic clinopyroxene miscibility gaps (e.g., Yokoyama and Sameshima, 1982; Matsumoto and Hirajima, 2005). However, the origin of omphacite remains controversial. Two miscibility gaps between omphacite and jadeite (e.g., Yokoyama and Sameshima, 1982; Tsujimori et al., 2005) and between omphacite and augite (e.g., Tsujimori and Liou, 2004) can occur. Previous studies (e.g., Black, 1970; Matsumoto and Banno, 1970; Carpenter, 1978; Zhang et al., 1999) revealed that different space groups can be adopted by omphacite (*P2/n*, *C2/c*, *P2/c*, *C2* and *P2*). Omphacite commonly crystallizes in the monoclinic system (space group *P2/n* or *C2/c*) with prismatic, typically twinned forms, though usually anhedral. Matsumoto and Banno (1970) first reported the *P2/n* space group for omphacite which is now the consensus among X-ray crystallographers (e.g., Cameron and Papike, 1981; Sasaki et al., 1981). Omphacite with space group *P2/n* is a cation-ordered pyroxene with two distinct M1 and two M2 sites, which can undergo a structural phase transition at high temperatures (Su et al., 2011). At temperatures above 800°C, omphacite is disordered with respect to its cations in M1 and M2 sites and exhibits space group *C2/c*. At temperatures below 800°C (depending on the composition), the cations Mg and Al convergently order on the M1 positions of the structure which leads to omphacite with space group *P2/n* (e.g., Carpenter, 1981; Putnis, 1992). Other studies (e.g., Godard and van Roermund, 1995; Bascou et al., 2001; Ulrich and Mainprice, 2005) showed that lattice preferred orientation of garnet typically displays randomly orientated patterns for eclogites, independent of metamorphic conditions or deformation processes, whereas omphacite is the main carrier of strain in these rocks. The Arquía Complex located in the Central Cordillera of the Colombian Andes has been widely studied in many cartographic, petrographic, lithostratigraphic and tectonic works (e.g., Grosse, 1926; Restrepo and Toussaint, 1974; Mosquera, 1978; Orrego et al., 1980a; Orrego et al., 1980b; McCourt et al., 1984; McCourt and Feininger, 1984; Murcia and Cepeda, 1991a; Murcia and Cepeda, 1991b; González, 1997; Ríos et al., 2008; Bustamante et al., 2011; García-Casco et al., 2011a; García-Casco et al., 2011b; Villagómez et al., 2011; Bustamante et al., 2012; Ruiz et al., 2012; García et al., 2017; Ríos et al., 2017). However, there are few publications focusing on high-pressure metamorphic rocks of the Central Cordillera, such as eclogites and their constituent minerals. In addition, there are no reports of any crystal structure determination of eclogitic minerals in Colombia. In the present work, we report microstructural, geochemical and crystallographic data of omphacite from an Arquía Complex eclogite. We propose a crystal-chemical and structural model for omphacite based on a combined characterization using scanning electron microscopy (SEM), electron probe microanalysis (EPMA) and single crystal X-ray diffraction (XRD).

MATERIALS AND METHODS

The analyzed omphacite comes from an eclogite sample from the Arquía Complex, cropping out between Pijao and Genova (Quindío), Central Cordillera, Colombian Andes. Mineral abbreviations used in the discussion are based on Whitney and Evans (2010). The omphacite-bearing eclogite was first analyzed by transmitted light microscopy, using an Olympus Trinocular BX51 microscope with a Nikon 5.5 Mpx camera and Nikon NIS Element-Br software. Photomicrographs were captured with a 5x objective. Secondary electron (SE) imaging and EDS analysis of omphacite were carried out using a FEI QUANTA 650 FEG-ESEM (field emission gun environmental scanning electron microscope), under the following analytical conditions: magnification = 700–100,000x, WD = 10.4 mm, HV = 25 kV, signal = SE mode, detector = BSED, EDS Detector EDAX APOLO X with resolution of 126.1 eV (in. Mn Kα). Major element compositions of omphacite were determined using a JEOL JXA 8800M electron probe microanalyzer, under the following analytical conditions: accelerating voltage 15 kV and probe current 20 nA (analysis) and 300 nA (mapping). Data acquisition and reduction were carried out using ZAF correction procedures. Natural and synthetic minerals were used as standards. Mineral compositions were determined by

TABLE 1 | Data collection and details of the structure refinement for omphacite.

Crystal data	
Structural formula	$(Ca_{0.173}Na_{0.328})^{M2}(Ca_{0.325}Na_{0.148})^{M21}(Mg_{0.464}Fe_{0.032})^{M1}(Al_{0.494}Fe_{0.006})^{M11}(Si_{1.95}Al_{0.05})O_6$
M (g/mol)	210.84
Crystal system	Monoclinic
Space group	*P*2/c (No. 13)
a (Å)	5.2627 (4)
b (Å)	8.7953 (6)
c (Å)	9.5316 (7)
β (°)	105.125 (8)
V (Å^3)	425.91 (6)
Z	4
Data collection	
Temperature (K)	293
Radiation (Å)	Mo Kα 0.71073
Theta Min-Max (°)	3.2–27.8
Dataset (°)	–6:5; –9:11; -12:12
Tot., Uniq. Data	3,367, 887
Observed Data [I > 2σ(I)]	801
R_{int}	0.028
Refinement	
Nref, Npar	887, 98
R, *wR* (F^2), *S*	0.0452, 0.1289, 1.12
Min. and Max. Resd. Dens. (Å^3)	–1.52, 0.6

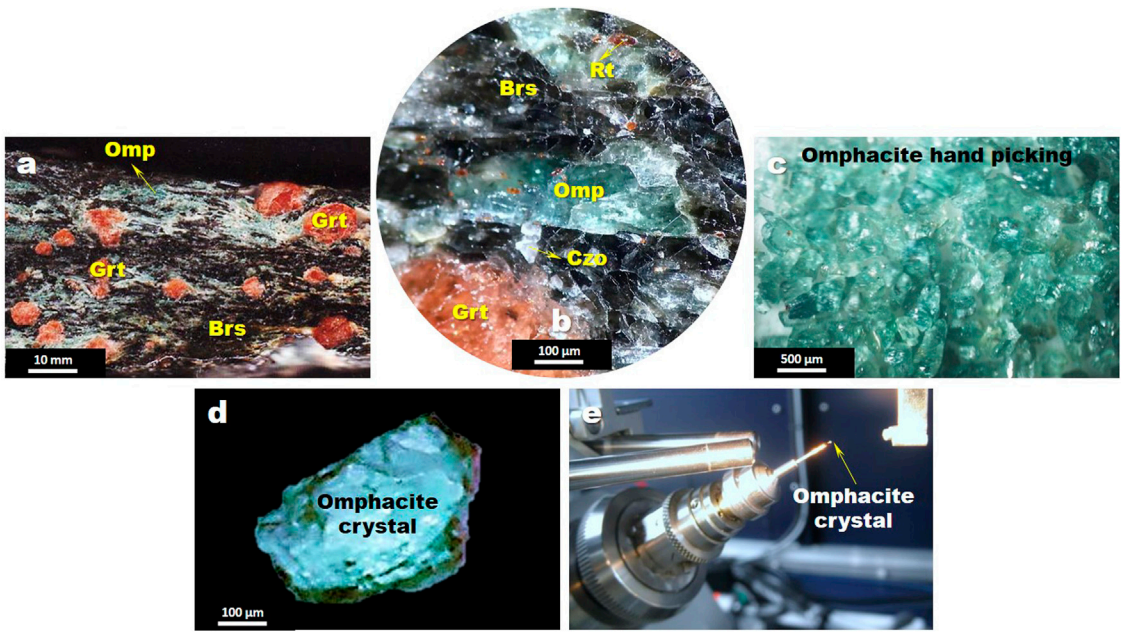

FIGURE 1 | (A,B) Macroscopic features of the analyzed omphacite-bearing eclogite showing the presence of omphacite (Omp), garnet (Grt), barroisite (Brs), clinozoisite (Czo), quartz (Qz), rutile (Rt). **(C)** Hand-picked omphacite crystals isolated from the eclogite. **(D)** Selected crystal fragment of omphacite used for single crystal data collection. **(E)** Omphacite crystal mounted on the diffractometer.

multiple spot analyses. The classification of clinopyroxene was carried out following the methodology of Essene and Fyfe (1967) and Morimoto (1988). Carbon coating was performed using a Cressington Carbon Coater 108C/Auto with a voltage of 115 V, 30 s, 0.1 mPa and 20 nm of thickness. A crystal fragment of dimensions 0.37 × 0.25 × 0.20 mm was selected for single-crystal X-ray diffraction. The unit-cell parameters and diffraction data were measured at room temperature using a single-crystal Rigaku XTALAB P200 three circle diffractometer equipped with graphite monochromated Mo Kα radiation (λ= 0.71073 Å, 50 kV and 40 mA) and a Pilatus 200 K area detector. The intensity data were collected using the CrystalClear program (Rigaku, 2015a) and the integration and data reduction were carried out with the

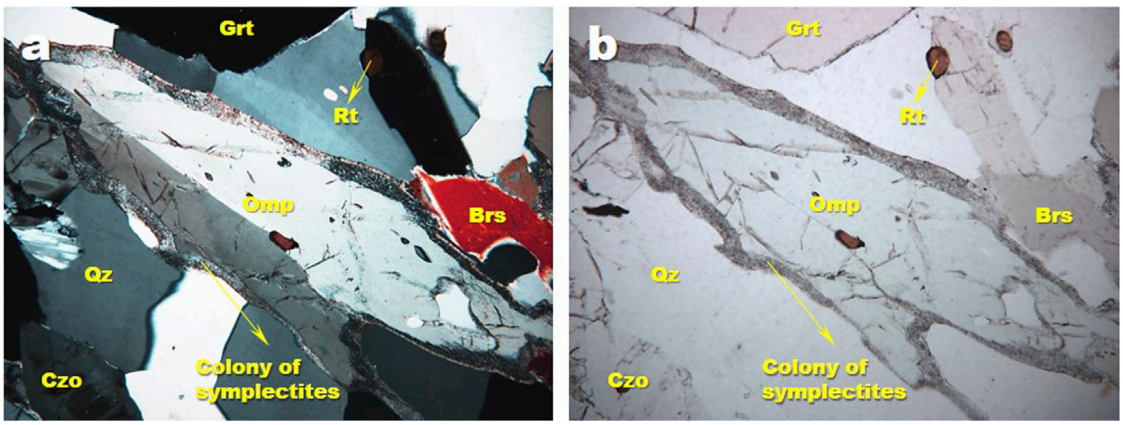

FIGURE 2 | Photomicrographs of the omphacite specimen observed under a transmitted light microscope with **(A)** cross polarized light and **(B)** plane light. The presence of omphacite (Omp), garnet (Grt), barroisite (Brs), clinozoisite (Czo), quartz (Qz) and rutile (Rt) is indicated.

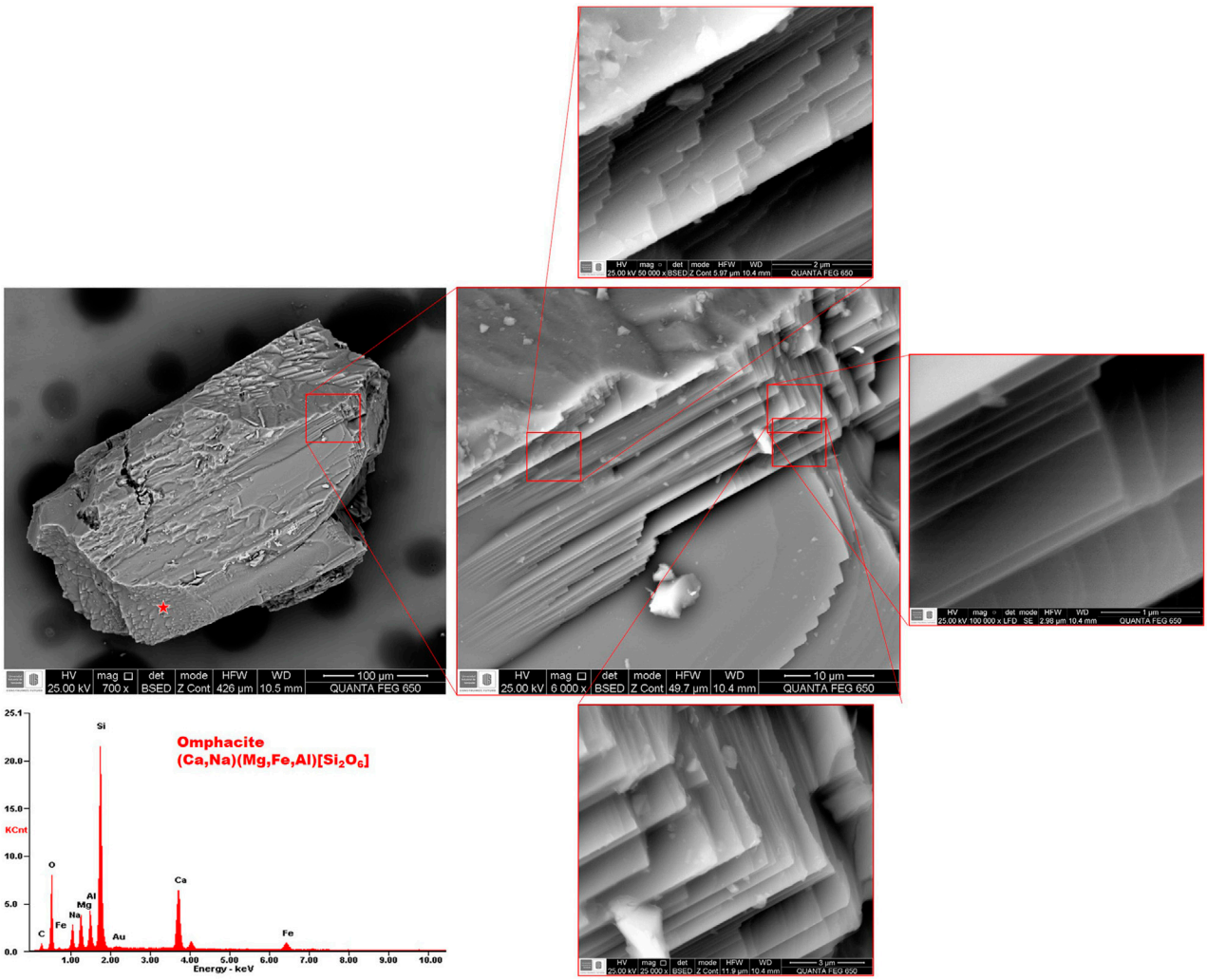

FIGURE 3 | SEM images in BSE mode along with the EDS spectrum of the studied omphacite.

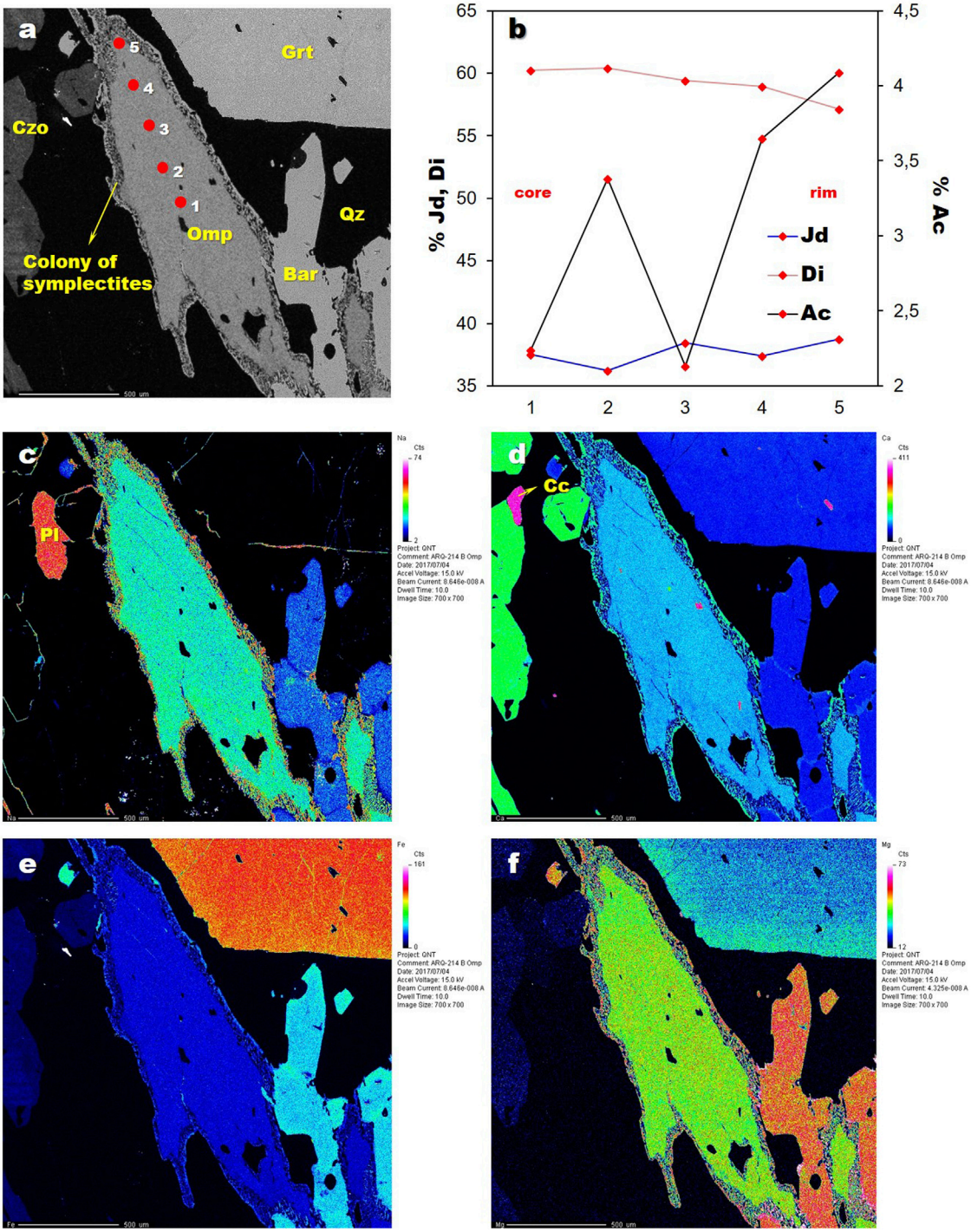

FIGURE 4 | (A) Back-scattered electron image of omphacite surrounded by a colony of symplectites, showing the spot reference for mineral composition analysis. **(B)** Compositional profile across omphacite from core to rim. **(C–F)** X-ray mapping of Na, Ca, Fe and Mg for omphacite. Red shows areas of high concentration, blue represents areas of low concentration and black represents areas of very low concentration. Omp, Omphacite; Grt, garnet; Brs, barroisite; Czo, clinozoisite; Qz, quartz.

CrysAlys Pro program (Rigaku, 2015b). The structure was solved with SHELXT (Sheldrick, 2015a) and refined by Least-Squares methods with SHELXL (Sheldrick, 2015b). Anisotropic atomic displacement parameters were refined for all atoms. The details of the data collection are given in **Table 1**.

TABLE 2 | Representative EPMA analyses of omphacite and symplectite in eclogite.

Lithology	Eclogite	Eclogite	Eclogite	Eclogite	Eclogite	Eclogite	Eclogite	Eclogite
Sample No	core				rim	fine	medium	coarse
Analysis No	1	2	3	4	5	sym	sym	sym
Weight %								
SiO_2	54.866	54.685	54.808	54.724	54.821	52.996	53.794	53.838
TiO_2	0.130	0.122	0.134	0.110	0.094	0.249	0.101	0.026
Al_2O_3	9.746	9.696	10.135	9.910	10.238	5.338	3.525	1.466
FeO*	3.734	3.622	3.796	3.866	3.898	4.849	5.036	5.221
MnO	0.012	0.011	0.044	0.011	0.030	0.040	0.038	0.020
MgO	9.3390	9.634	9.253	9.325	9.028	12.258	13.093	13.874
CaO	16.051	16.297	15.785	15.880	15.425	21.880	22.218	23.847
Na_2O	5.562	5.509	5.645	5.726	6.025	2.062	1.611	1.202
K_2O	0.000	0.000	0.001	0.000	0.007	0.000	0.000	0.000
Cr_2O_3	0.025	0.023	0.013	0.027	0.032	0.083	0.114	0.048
Total	99.25	99.60	99.62	99.58	99.60	99.76	99.53	99.54
Numbers of ions on the basis of 6 O								
Si	1.972	1.966	1.968	1.968	1.969	1.942	1.977	1.992
Al^{IV}	0.028	0.034	0.032	0.032	0.031	0.058	0.023	0.008
Sum T	2.000	2.000	2.000	2.000	2.000	2.000	2.000	2.000
Al^{VI}	0.385	0.377	0.396	0.388	0.403	0.173	0.130	0.056
Fe^{3+}	0.023	0.035	0.022	0.038	0.043	0.017	0.002	0.036
Cr	0.001	0.001	0.000	0.001	0.001	0.002	0.003	0.001
Ti	0.003	0.003	0.004	0.003	0.003	0.007	0.003	0.001
Mg	0.503	0.516	0.495	0.500	0.483	0.670	0.717	0.765
Fe^{2+}	0.089	0.074	0.092	0.078	0.075	0.131	0.153	0.125
Mn	0.000	0.000	0.001	0.000	0.001	0.001	0.001	0.001
Ca	0.618	0.628	0.607	0.612	0.594	0.859	0.875	0.945
Na	0.388	0.384	0.393	0.399	0.420	0.147	0.115	0.086
K	0.000	0.000	0.000	0.000	0.000	0.000	0.000	0.000
Sum M1,M2	2.011	2.017	2.011	2.019	2.021	2.008	1.999	2.017
Total	4	4	4	4	4	4	4	4
Jd	37.53	36.23	38.45	37.38	38.77	14.32	11.58	5.41
Ac	2.24	3.38	2.13	3.65	4.09	1.70	0.19	3.50
Di	60.23	60.39	59.42	58.97	57.14	83.98	88.23	91.09
X_{Fe}	0.21	0.32	0.19	0.33	0.36	0.11	0.01	0.22

**Total Fe as FeO + Fe_2O_3.*
Sym, symplectite.

RESULTS

Omphacite Microstructural Description

The retrograde host eclogite (**Figure 1A**) exhibits a general banded structure, from millimeters to a couple of centimeters, varying from continuous to discontinuous, with a clearly defined metamorphic foliation direction. These features are mainly defined by the distribution of the omphacite (green color) and by barroisite type amphibole (dark green color), generated by retrogradation. Garnets vary from equigranular to inequigranular and are predominantly red-orange in color, giving the rock a nodular structure, with an average diameter of 5 mm. Omphacite shows a prismatic to laminar habit, exfoliable, with a translucent grass green color and a characteristic vitreous luster. It is surrounded by asymmetric crowns of matt green symplectites (**Figure 1B**) and associated with barroisite, rutile and clinozoisite. **Figure 1C** shows a hand-picked fraction of omphacite from the analyzed eclogite. The omphacite crystal selected for single crystal X-ray diffraction analysis is shown in **Figure 1D** and **Figure 1E** shows the crystal mounted in the diffractometer.

Petrographically, omphacite is abundant in the less retrograde eclogites (25%) and occurs in the rock matrix as separate individuals of subidioblastic to xenoblastic character or in leafy and exfoliable aggregates, with inclusions of rutile, clinozoisite and quartz. It is commonly observed rimmed by symplectitic intergrowths or as a relict partially or totally included in amphibole. **Figure 2** shows a polysynthetic twinned omphacite blast. Note the occurrence of a symplectitic texture around omphacite, which contains inclusions of rutile and quartz. Omphacite is associated to garnet, quartz, barroisite and clinozoisite.

Retrograde eclogites of the Arquía Complex generally show a geochemical behavior similar to tholeiitic basalts, mid-oceanic ridge basalt (MORB) and, more exactly, normal N-MORB, in agreement with reports by several authors (e.g., Pearce, 1982; Pearce, 2008; Meschede, 1986; Hastie et al., 2007). According to Castellanos (2021), the eclogites had to complete their equilibrium stage at a P-T peak in which the omphacite-garnet assembly was stabilized. These two index mineral phases are observed in net contact without the development of

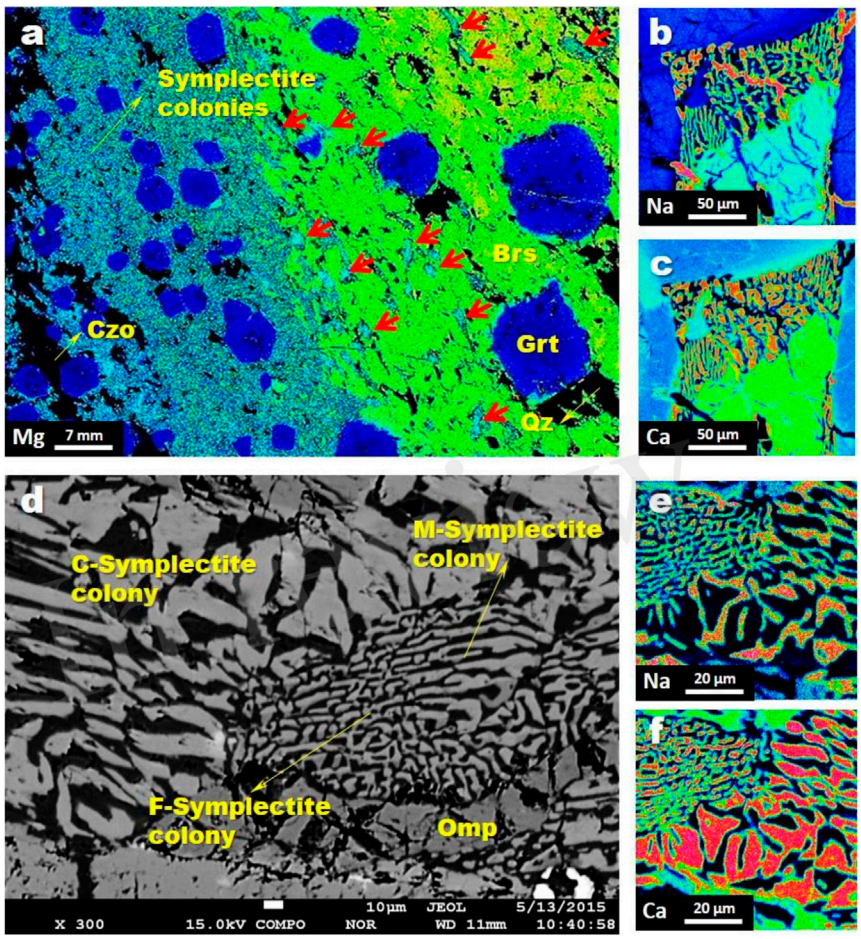

FIGURE 5 | Chemical composition and textural features of omphacite and associated symplectites. **(A–C)** chemical distribution of Mg, Na, and Ca, respectively. **(D–F)** show coarse (C), medium (M) and fine (F) textural features of the symplectite colonies.

intergranular phases. The appearance of the garnet + omphacite assembly depends on the Ca/Na ratio and the total Na_2O content, so that as the pressure increases, the Ca/Na ratio decreases progressively, and albite is stabilized at conditions of low pressure. Likewise, the orthopyroxene disappears at conditions that depend on the Fe/Mg ratio, as the solid garnet solution expands towards compositions richer in pyrope, which impedes the stability of the orthopyroxene within the assembly.

Omphacite Morphology and Composition

SEM images of the analyzed omphacite grain are shown in **Figure 3**. Omphacite shows two planes of cleavage in two {110} directions at nearly right angles (87° and 93°) to the **c**-axis [on (001)].

The EDS spectrum reveals that omphacite is mainly composed of O (32.30 wt%.), Si (30.46 wt%.), Ca (10.82 wt%.), Al (5.45 wt %.), Mg (5.16 wt%.), Na (4.75 wt%.), with minor amounts of Fe (2.92 wt%.) and Au (1.02 wt%.). The C peak is attributed to carbon coating.

Figures 4A,B show a back-scattered electron image and a compositional profile across omphacite, which is acmite-poor (2.13–4.09%) and diopside-rich (57.14–60.39%). It usually lacks compositional zoning and therefore it is almost chemically homogenous with the exception of the jadeite content {100 $[(2Na/(2Na + Ca + Mg + Fe^{2+}))\ (Al_{M1}/(Al_{M1}+Fe^{3+}_{M1}))]$}, which shows a slight increase from core ($Jd_{36.23\text{-}37.53}$) to rim ($Jd_{38.38\text{-}38.77}$). **Figures 4C–F** show the X-ray mapping of Na, Ca, Fe and Mg for Omphacite. The original mineral paragenesis with garnet and quartz is preserved and appears spatially associated with other mineral phases (plagioclase, barroisite, clinozoisite and calcite) that correspond to the retrograde metamorphism process. Omphacite shows medium Mg-concentration, medium to low Na- and Ca-concentration, and low Fe-concentration. We confirm that the chemical homogeneity of omphacite is probably due to reaching equilibrium at the peak PT conditions. Microtextural analysis reveals that the colonies of symplectites of the analyzed sample are morphologically similar to those described in previous studies (e.g., Mysen and Griffin, 1973; Boland and van Roermund, 1983; Anderson and Moecher, 2007; Su et al., 2011; Moulas et al., 2015). The symplectite formation is promoted in quartz-bearing eclogites unlike other contexts (quartz-free eclogites) in which this process may require

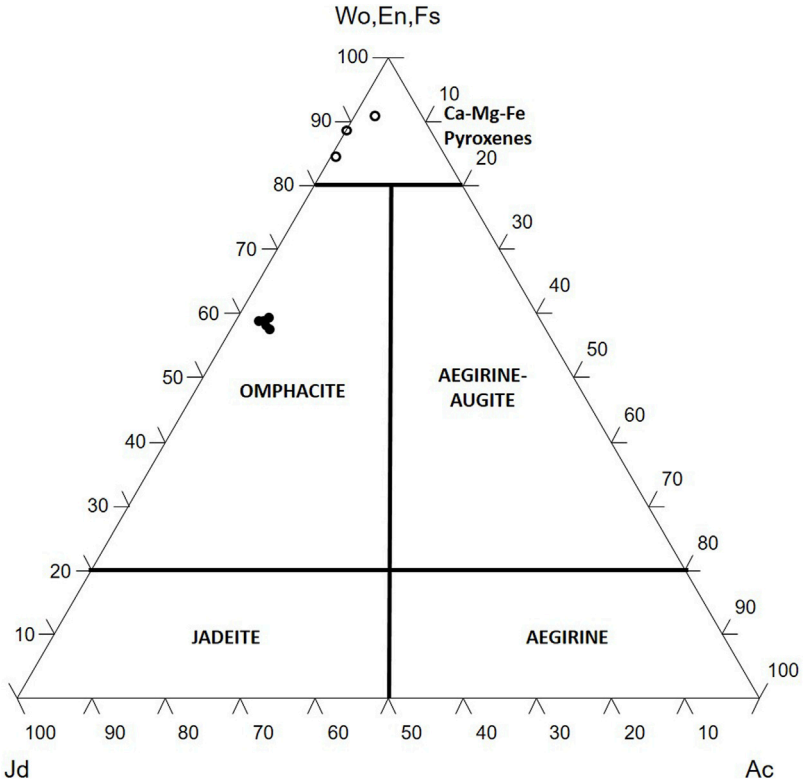

FIGURE 6 | Triangular plot showing the compositional field of omphacite from retrograde eclogites. Jd, jadeite; Ac, acmite; Wo, wollastonite; En, Enstatite; Fs, Ferrosilite.

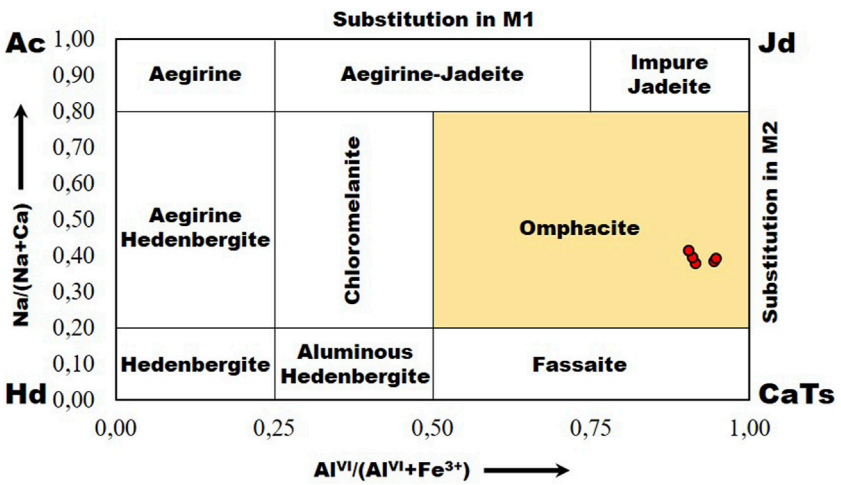

FIGURE 7 | Classification proposed for alkaline pyroxenes, incorporating the field of omphacite as defined by Clark and Papike (1968). Ac, acmite; Hd, hedenbergite; Jd, jadeite; CaTs, Ca tschermakite.

intergranular transport of silica in a fluid phase or oxidation of omphacite (Mysen and Griffin, 1973). According to Mysen and Griffin (1973), either the original omphacite or the colony of symplectites are non-stoichiometric or the exsolution process has involved metasomatic exchange of material between the omphacite and its surroundings. The presence of symplectites after omphacite indicates a drop in pressure from 17.5 to 8 kbar (Castellanos, 2021).

Table 2 shows representative chemical compositions of omphacite and associated symplectites. The calculation of the

TABLE 3 | Atomic coordinates and equivalent isotropic displacement parameters of the non-hydrogen atoms in the omphacite structure.

Atom	*x*	*y*	*z*	Ueq Å^2
M1	0	-0.15912 (8)	1/4	0.0051 (3)
M11	1/2	0.65297 (8)	1/4	0.0052 (3)
M2	1/2	–0.04977 (7)	3/4	0.0109 (3)
M21	1	0.55207 (9)	3/4	0.0097 (3)
T1	0.68802 (11)	0.34685 (6)	0.46098 (5)	0.0073 (3)
T2	0.19335 (10)	0.16214 (6)	0.46282 (5)	0.0069 (3)
O1	0.2000 (3)	–0.00169 (17)	0.39293 (14)	0.0117 (4)
O2	–0.1015 (3)	0.23927 (16)	0.40154 (14)	0.0097 (4)
O3	0.3961 (3)	0.26699 (16)	0.39405 (13)	0.0092 (4)
O4	0.7607 (3)	0.33901 (13)	0.63682 (15)	0.0109 (4)
O5	0.6960 (3)	0.50855 (16)	0.38524 (14)	0.0106 (4)
O6	0.2867 (3)	0.17642 (13)	0.63833 (15)	0.0105 (4)

structural formula was based on 6 oxygens and 4 cations. For the blasts in the matrix of retrograde eclogites, the jadeite content varies between 37.38 and 38.77 wt%. The Na content increases slightly from core (0.388 wt%) to rim (0.420 wt%). The Ca content decreases slightly from core (0.618 wt%) to rim (0.594 wt%). The X_{Fe} varies between 0.19 and 0.36, although these zonal variations are not graphically observed in the color compositional maps. For the clinopyroxene of the symplectites, the jadeite content varies between 5.41 and 14.32 wt%. The Na content varies between 0.086 and 0.115 wt%, the Ca content varies between 0.859 and 0.945 wt%, and the X_{Fe} varies between 0.01 and 0.22. These data indicate that omphacite-type pyroxene composes the matrix whereas sodium augite-type composes the symplectites.

Figure 5A illustrates an elemental distribution map for Mg corresponding to a retrograde eclogite, with garnet porphyroblasts (in blue) associated with omphacite (in light blue) and amphibole type Mg-katophorite (in lemon green). The transition omphacite → symplectite presents all characteristics of a discontinuous precipitation reaction (e.g., Boland and van Roermund, 1983; Joanny et al., 1989). It is worth noting the occurrence of clinozoisite and quartz in the matrix, which are also black in color. **Figures 5B,C** show the elemental distribution maps for Na and for Ca, respectively, which illustrate an omphacite blast rimmed by a colony of symplectites. **Figure 5D** is a BSE image of a symplectite colony exhibiting a textural change with c-coarse, m-medium and f-fine varieties. **Figures 5E,F** illustrate the relationship between plagioclase, amphibole and pyroxene in Na and Ca color maps. Other features such as retrogradation textures can be seen in the elemental distribution maps for Na and Ca (**Figures 5E,F**). They reveal the occurrence of three textural types of symplectites, with the presence of fine-grained symplectites (<10 μm) in the upper left corner, medium-grained symplectites (30 μm) in the upper right corner, and coarse-grained symplectites (>50 μm) in the lower part. The change in the textural features of the symplectites probably reflects changes in temperature conditions. The chemical composition of omphacite in retrograde eclogites is shown in **Figure 6**. It varies from omphacite to sodium augite. **Figure 7** illustrates the omphacite compositional field within the aluminous and ferric clinopyroxenes (Clark and Papike, 1968).

Single-Crystal X-Ray Diffraction

Omphacite crystallizes in the monoclinic space group *P*2/*c* (No. 13) with the following unit cell parameters: $a = 5.2627$ (4) Å, $b = 8.7953$ (6) Å, $c = 9.5316$ (7) Å, $\beta = 105.125$ (8)° and $V = 425.91$ (6) Å^3, Z = 4. Crystallographic data are shown in **Table 1**. Fractional atomic coordinates and equivalent isotropic displacement parameters for omphacite are presented in **Table 3**, while the interatomic distances and the selected angles are shown in **Table 4**. It must be mentioned that the structure can also be refined successfully in space group *P*2/*a*. Space group *P*2/*c* was selected as it is customarily considered the standard setting.

The *P*2/*c* space group reported in this study for omphacite is consistent with the possible space groups previously reported for this mineral. It can be interpreted as an intermediate description of a sliding replacement reaction whose final equilibrium would be described in space group *P*2/*n* (e.g., Carpenter, 1979). Therefore, it cannot be considered the same as the omphacite described by several authors (e.g., Matsumoto et al., 1975; Smith et al., 1980; Rossi et al., 1983; Mottana et al., 1997; Matsumoto and Hirajima, 2005; Moghadam et al., 2010; McNamara, 2012; Pandolfo et al., 2012; Xie et al., 2020), who concluded that the only permitted space group for primitive (ordered) omphacite is *P*2/*n*, which has 2M2, 2M1 and 2T individual cation sites.

The refinement of the structure was carried out using constraints based on the results of the chemical analysis. The chemical parameters considered were the atomic fractions of Al^{3+}, Mg^{2+}, Fe^{2+}, Fe^{3+}, Ca^{2+}, and Na^{+} determined with the EDS facilities attached to the Scanning Electron Microscope. Elements such as Ti, Cr, and Mn were not considered as they do not exceed 0.005 atoms per formula unit (apfu) and their sum does not exceed 0.009 apfu in the analyzed sample. It was assumed that all the positions were fully occupied. The Ca and Na atoms were located at the M2 and M21 sites while the Mg and Al atoms were located in the M1 and M11 sites. The Fe^{2+} content was determined based on the residual electron density needed to achieve complete occupation of both M1 sites. The chemical formula obtained after the structural refinement process was $(Ca_{0.173}Na_{0.328})^{M2}(Ca_{0.325}Na_{0.148})^{M21}(Mg_{0.464}Fe_{0.032})^{M1}(Al_{0.494}Fe_{0.006})^{M11}(Si_{1.95}Al_{0.05})O_6$.

The omphacite site populations obtained from the structural refinement results were used to calculate the long-range order parameters Q^{occ}_{M1} and Q^{occ}_{M2} for the M1 and M2 sites shown in **Table 5** using **Eq. 1** and **Eq. 2** (Carpenter et al., 1990). The order parameters expressed in terms of mean bond lengths (Q^{dist}_{M1} and Q^{dist}_{M2}) were calculated using the mean bond length of the octahedra and polyhedra (**Eq. 3** and **Eq. 4**) as suggested by Carpenter et al. (1990).

$$Q^{occ}_{M1} = \frac{\left|\frac{\left(Al+Fe^{3+}\right)_{M1}-\left(Al+Fe^{3+}\right)_{M11}}{\sum\left(Al+Fe^{3+}\right)}\right| + \left|\frac{\left(Mg+Fe^{2+}\right)_{M1}-\left(Mg+Fe^{2+}\right)_{M11}}{\sum\left(Mg+Fe^{2+}\right)}\right|}{2} \quad (1)$$

TABLE 4 | Selected bond distances (Å) and angles (°) for omphacite.

Atoms	Bond distance (Å)	Atoms	Bond angle (°)	Atoms	Bond angle (°)	Atoms	Bond angle (°)
Fe1-O1	2.0329 (15)	O1-Fe1-O1^{I}	94.14 (6)	O1^{I}-Mg1-O4^{V}	91.85 (6)	O4^{VI}-Al1-O6^{VIII}	83.67 (6)
Fe1-O1^{I}	2.0329 (15)	O1-Fe1-O6^{II}	91.43 (6)	O1^{I}-Mg1-O6^{VII}	91.43 (6)	O4^{VIII}-Al1-O6^{VI}	83.67 (6)
Fe1-O6^{II}	2.0666 (16)	O1-Fe1-O4^{III}	91.85 (6)	O4^{III}-Mg1-O6^{II}	95.68 (6)	O6^{VI}-Al1-O6^{VIII}	83.11 (6)
Fe1-O4^{III}	2.1317 (14)	O1-Fe1-O4^{V}	168.20 (6)	O4^{V}-Mg1-O6^{II}	77.98 (6)	O1-Mg1-O4^{V}	168.20 (6)
Fe1-O4^{V}	2.1317 (14)	O1-Fe1-O6^{VII}	94.32 (6)	O6^{II}-Mg1-O6^{VII}	171.56 (6)	O1-Mg1-O6^{VII}	94.32 (6)
Fe1-O6^{VII}	2.0666 (16)	O1^{I}-Fe1-O6^{II}	94.32 (6)	O4^{III}-Mg1-O4^{V}	84.16 (6)	O1^{I}-Mg1-O6^{II}	94.32 (6)
Fe2-O5	1.9092 (15)	O1^{I}-Fe1-O4^{III}	168.20 (6)	O4^{III}-Mg1-O6^{VII}	77.98 (6)	Si1^{XII}-O2-Si2	139.39 (9)
Fe2-O5^{IV}	1.9092 (15)	O1^{I}-Fe1-O4^{V}	91.85 (6)	O4^{V}-Mg1-O6^{VII}	95.68 (6)	Si1^{XII}-O2-Al2	139.39 (9)
Fe2-O4^{VI}	1.9554 (16)	O1^{I}-Fe1-O6^{VII}	91.43 (6)	O1-Mg1-O1^{I}	94.14 (6)	Si1-O3-Si2	134.94 (8)
Fe2-O6^{VI}	2.0053 (14)	O4^{III}-Fe1-O6^{II}	95.68 (6)	O1-Mg1-O6^{II}	91.43 (6)	Si1-O3-Al2	134.94 (8)
Fe2-O4^{VIII}	1.9554 (16)	O4^{V}-Fe1-O6^{II}	77.98 (6)	O1-Mg1-O4^{III}	91.85 (6)	Fe1^{III}-O4-Si1	120.26 (8)
Fe2-O6^{VIII}	2.0053 (14)	O6^{II}-Fe1-O6^{VII}	171.56 (6)	O6^{VI}-Fe2-O6^{VIII}	83.11 (6)	Si1-O4-Mg1^{III}	120.26 (8)
Si1-O3	1.6580 (16)	O4^{III}-Fe1-O4^{V}	84.16 (6)	O4^{VIII}-Fe2-O6^{VIII}	93.23 (6)	Fe2^{VI}-O4-Si1	123.98 (9)
Si1-O4	1.6204 (15)	O4^{III}-Fe1-O6^{VII}	77.98 (6)	O3-Si1-O4	108.96 (8)	Si1-O4-Al1^{VI}	123.98 (9)
Si1-O5	1.6004 (15)	O4^{V}-Fe1-O6^{VII}	95.68 (6)	O3-Si1-O5	109.49 (8)	Fe2^{X}-O4-Si1	123.98 (9)
Si1-O2^{IX}	1.6646 (16)	O5-Fe2-O5^{IV}	96.59 (7)	O2^{IX}-Si1-O3	105.09 (8)	Si1-O4-Al1^{X}	123.98 (9)
Si2-O1	1.5917 (16)	O4^{VI}-Fe2-O5	89.13 (6)	O4-Si1-O5	118.52 (7)	Fe1^{XI}-O4-Si1	120.26 (8)
Si2-O2	1.6541 (16)	O5-Fe2-O6^{VI}	90.60 (6)	O2^{IX}-Si1-O4	109.23 (8)	Si1-O4-Mg1^{XI}	120.26 (8)
Si2-O3	1.6684 (16)	O4^{VIII}-Fe2-O5	93.63 (6)	O2^{IX}-Si1-O5	104.68 (8)	Fe2-O5-Si1	145.35 (10)
Si2-O6	1.6207 (15)	O5-Fe2-O6^{VIII}	170.13 (6)	O1-Si2-O2	110.15 (8)	Si1-O5-Al1	145.35 (10)
Al1-O5	1.9092 (15)	O4^{VI}-Fe2-O5^{IV}	93.63 (6)	O1-Si2-O3	104.47 (8)	Fe2^{IV}-O5-Si1	145.35 (10)
Al1-O5^{IV}	1.9092 (15)	O5^{IV}-Fe2-O6^{VI}	170.13 (6)	O1-Si2-O6	117.92 (7)	Si1-O5-Al1^{IV}	145.35 (10)
Al1-O4^{VI}	1.9554 (16)	O4^{VIII}-Fe2-O5^{IV}	89.13 (6)	O2-Si2-O3	105.77 (8)		
Al1-O6^{VI}	2.0053 (14)	O5^{IV}-Fe2-O6^{VIII}	90.60 (6)	O2-Si2-O6	109.66 (8)		
Al1-O4^{VIII}	1.9554 (16)	O4^{VI}-Fe2-O6^{VI}	93.23 (6)	O3-Si2-O6	108.06 (7)		
Al1-O6^{VIII}	2.0053 (14)	O4^{VI}-Fe2-O4^{VIII}	175.87 (6)	O5-Al1-O5^{IV}	96.59 (7)		
Al2-O2	1.6541 (16)	O4^{VI}-Fe2-O6^{VIII}	83.67 (6)	O4^{VI}-Al1-O5	89.13 (6)		
Al2-O3	1.6684 (16)	O4^{VIII}-Fe2-O6^{VI}	83.67 (6)	O5-Al1-O6^{VI}	90.60 (6)		
Al2-O6	1.6207 (15)	O4^{VIII}-Al1-O6^{VIII}	93.23 (6)	O4^{VIII}-Al1-O5	93.63 (6)		
Al2-O1	1.5917 (16)	O1-Al2-O2	110.15 (8)	O5-Al1-O6^{VIII}	170.13 (6)		
Mg1-O4^{V}	2.1317 (14)	O1-Al2-O3	104.47 (8)	O4^{VI}-Al1-O5^{IV}	93.63 (6)		
Mg1-O6^{VII}	2.0666 (16)	O1-Al2-O6	117.92 (7)	O5^{IV}-Al1-O6^{VI}	170.13 (6)		
Mg1-O4^{III}	2.1317 (14)	O2-Al2-O3	105.77 (8)	O4^{VIII}-Al1-O5^{IV}	89.13 (6)		
Mg1-O1	2.0329 (15)	O2-Al2-O6	109.66 (8)	O5^{IV}-Al1-O6^{VIII}	90.60 (6)		
Mg1-O1^{I}	2.0329 (15)	O3-Al2-O6	108.06 (7)	O4^{VI}-Al1-O6^{VI}	93.23 (6)		
Mg1-O6^{II}	2.0666 (16)	O1^{I}-Mg1-O4^{III}	168.20 (6)	O4^{VI}-Al1-O4^{VIII}	175.87 (6)		

Symmetry Code: (I) = -x, y, 1/2-z; (II) = -x, -y, 1-z; (III) = 1-x, -y, 1-z; (IV) = 1-x, y, 1/2-z; (V) = -1+x, -y, -1/2 + z; (VI) = 1-x, 1-y, 1-z; (VII) = x, -y,- 1/2 + z; (VIII) = x, 1-y, -1/2 + z; (IX) = 1 + x, y, z; (X) = x, 1-y, 1/2 + z; (XI) = 1 + x, -y, 1/2 + z; (XII) = -1+x, y, z.

TABLE 5 | Site populations and degree of order for omphacite.

T1	Si1	1.000	M2	Ca2	0.3460
T2	Si2	0.950		Na2	0.6560
	Al2	0.050	M21	Ca1	0.7040
M1	Mg1	0.937		Na1	0.2960
	Fe1	0.063	Q^{occ}_{M1}		1.0000
M11	Al1	0.987	Q^{occ}_{M2}		0.3595
	Fe2	0.013	Q^{dist}_{M1}		0.05981
			Q^{dist}_{M2}		0.01489

$$Q^{occ}_{M1} = \frac{\left|\frac{Na_{M2}-Na_{M21}}{\sum Na}\right| + \left|\frac{Ca_{M2}-Ca_{M21}}{\sum Ca}\right|}{2} \quad (2)$$

$$Q^{dist}_{M1} = \left|\frac{\langle M_1 - O\rangle - \langle M_{11} - O\rangle}{\frac{1}{2}\left(\langle M_1 - O\rangle + \langle M_{11} - O\rangle\right)}\right| \quad (3)$$

$$Q^{dist}_{M2} = \left|\frac{\langle M_2 - O\rangle - \langle M_{21} - O\rangle}{\frac{1}{2}\left(\langle M_2 - O\rangle + \langle M_{21} - O\rangle\right)}\right| \quad (4)$$

Figure 8 shows a projection of the omphacite structure along the **c**-axis. The M1 site is occupied by Mg^{2+} and Fe^{2+} while the M11 site is occupied by Al^{3+} and Fe^{3+}, both with octahedral coordination. On the other hand, the M2 and M21 sites with coordination-8 are occupied by Ca and Na. Two types of tetrahedral sites are present in the structure: T1 entirely occupied by Si and T2 with Si and Al. O2 and O3 oxygens are bridging atoms attached to silicon atoms, while O1 is attached to the M1 octahedron and O5 to the M11 octahedron. The difference between the two tetrahedra in the structure is slight, in accord with Matsumoto et al. (1975). The Si-O bonds involving the bridging oxygens [O3(l) and O3 (2)] are significantly longer than those to other nonbridging oxygens, as in other clinopyroxenes. The angle O1-Si-O2 is 118° for each tetrahedron, compared with 105° for O2-Si-O3, reflecting the long O1 (1)-O2 (1) and O1 (2)-O2 (2) distances of 2.757 and 2.742 Å, respectively. The angle O2-O3-O2 is used as a measure of the extension of the silicate chain. Since its value of 169.002 (2)° (**Table 6**) is within the 150°–210° range, a sequence of layers of almost straight and slightly twisted silicon tetrahedra chains can

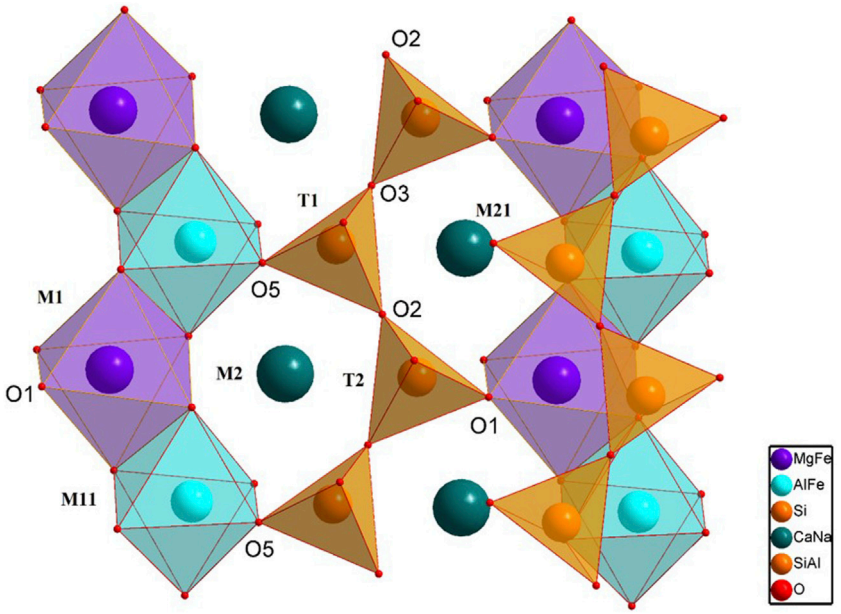

FIGURE 8 | Projection of the structure of omphacite viewed along the **c**-axis.

TABLE 6 | Bond distances, polyhedral volumes, quadratic elongation (TQE), bond angle variance (BAV) and other geometrical parameters for omphacite.

T1-O2	1.6646 (16)	T2-O1	1.59170 (10)
T1-O3	1.6580 (16)	T2-O2	1.65418 (13)
T1-O4	1.6204 (15)	T2-O3	1.66862 (10)
T1-O5	1.6004 (15)	T2-O6	1.62066 (14)
<T1-O>	1.6358	<T2-O>	1.6338
V (Å^3)	2.2280	V (Å^3)	2.2214
TQE	1.0057	TQE	1.0053
BAV(°)	24.8694	BAV(°)	22.5568
TILT(°)	3.33	TILT(°)	1.84
M1-O1	2.03296 (13)	M11-O4	1.95519 (15)
M1-O4	2.13181 (13)	M11-O5	1.90922 (13)
M1-O6	2.06651 (16)	M11-O6	1.90922 (13)
<M1-O>	2.0771	<M11-O>	1.9566
V (Å^3)	11.7316	V (Å^3)	9.9006
OQE	1.0127	OQE	1.0062
OAV(°)	41.2278	OAV(°)	20.0467
M2-O2	2.36270 (17)	M22-O1	2.38237 (18)
M2-O3	2.69637 (19)	M22-O2	2.7715 (2)
M2-O4	2.35642 (14)	M22-O3	2.49506 (13)
M2-O5	2.36270 (17)	M22-O6	2.39327 (14)
<M2-O>	2.4735	<M21-O>	2.5106
V (Å^3)	24.8376	V (Å^3)	26.0269
O2-O3-O2	169.002 (2)°	O5-O1-O5	62.831 (1)°

be identified (Cameron and Papike, 1981). The M1 and M11 octahedra share edges to form zigzag chains parallel to the **a**-axis while M2 and M21 polyhedra lie diagonally to the octahedron´s sides.

Bond angle variance (σ2) and quadratic elongation (λ) are employed to describe the deviation from the ideal polyhedral shape (Robinson et al., 1971). According to Rossi et al. (1983), some geometrical features of the tetrahedra as well as of the octahedra (e.g., tetrahedral quadratic elongation and TILT angle) are not a simple linear function of composition, even when no change in space group occurs.

DISCUSSION

Na-pyroxene omphacite is a high-pressure mineral index of the eclogite metamorphic facies. According to previous studies (e.g., Maresch and Abraham, 1981; Bakirov et al., 1998; Miyagi and Takasu, 2005; Kabir and Takasu, 2010; Arrieta-Prieto et al., 2020), the average Na content in "fresh" eclogites worldwide is about 8.0 wt%, whereas in the present study we report an average Na content of 5.0 wt%. This fact could be interpreted as a product of the intense retrogradation and chemical imbalance exhibited by the Arquía Complex, which in light of these results becomes a highly limiting factor in geochemical, thermobarometric and geochronological models.

Depending on the crystallization conditions, omphacite can adopt one of two different crystal structures: the substitutionally-disordered high-temperature phase with space group *C2/c* and the cation-ordered phase with space group *P2/n* (e.g., Moghadam et al., 2010; McNamara, 2012). The structure of the pyroxene studied here is consistent with omphacite with ordered cations although the structure is better described in space group *P2/c*. The chains along the **c**-axis, formed by the M1 and M11 octahedra that share edges, alternate with M1 (Mg^{2+}, Fe^{2+}) and M11 (Al^{3+}, Fe^{3+}) octahedra. The larger volume M2 polyhedra link the octahedral chains in layers occupied by Na^{+} or Ca^{2+} cations. The adjacent layers along the **a** direction stack so that the M1 octahedron of one layer has an M11 octahedron above in the next layer and a similar zig-zag staggered arrangement prevails for M2

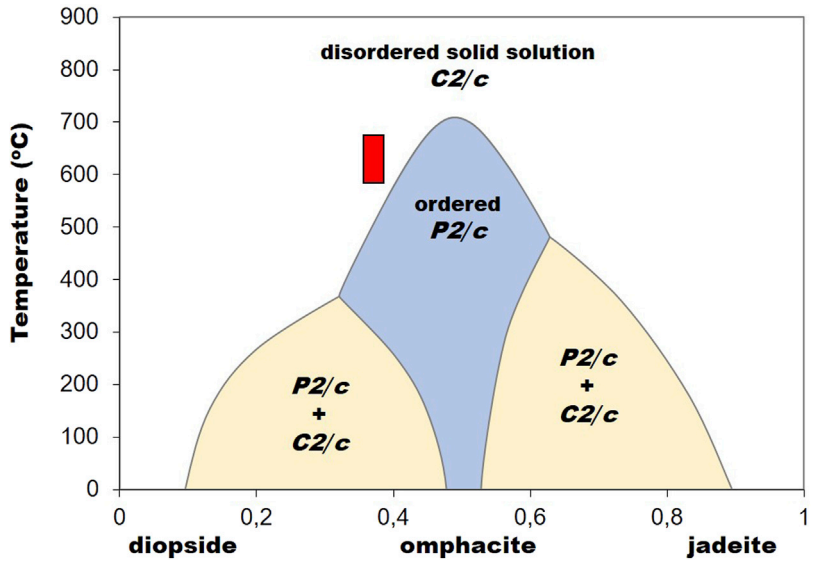

FIGURE 9 | Phase diagram for the jadeite-diopside system (adapted and modified after Carpenter, 1981). The red box indicates jadeite content in omphacite and calculated equilibrium temperatures according to Holland and Powell (2003).

polyhedra. The two crystallographically distinct silicate tetrahedra are joined to form the two chains of slightly distorted tetrahedra.

In general, omphacites from geological contexts where exhumation proceeds slowly tend to be of the *P2/n* variety (Zhang et al., 2016). Omphacite can be used as geothermometer (e.g., Råheim and Green, 1974) and geobarometer (e.g., Zhang, 1998), taking into account its temperature sensitivity of cation distribution and thermoelastic properties, respectively. Castellanos (2021) reports the occurrence of eclogites in the Arquía Complex, which are primarily composed of omphacite and garnet. We consider omphacite as an intermediate phase in the diopside-jadeite solid solution system as reported in previous studies (e.g., Vinograd et al., 2007; Moghadam et al., 2010; Zhang et al., 2016). According to the phase diagram for the jadeite-diopside system shown in **Figure 9**, with increasing temperature, omphacite undergoes a phase transformation from the ordered structure with space group *P2/n* to the disordered *C2/c* structure. However, the analyzed omphacite shows a cation-ordered structure with space group *P2/c*, as evidenced by single-crystal X-ray diffraction, which reflects temperature conditions of formation below 800°C.

According to Skelton and Walker (2015), omphacite can show partial coupled substitution of (Na, Al)-(Mg-Fe, Ca), developing a relatively low symmetry space group *P2/n*. As temperature increases above ~800°C, the movements of the atoms increase, rendering a structure that displays disorder in the cationic sublattice. The space group of the disordered structure becomes *C2/c* (Fleet et al., 1978).

Omphacite shows a jadeite content of 0.36–0.39. Based on the Holland and Powell (2003) geothermometer, the calculated equilibrium temperature of its formation is in the range of 585–671°C, which suggests a disordered structure for omphacite (**Figure 9**). This is not in accordance with the results obtained in the present study using single-crystal X-ray diffraction. Several authors (e.g., Arlt et al., 1998; Ross and Reynard, 1999) have suggested that, with increasing pressure, there is a first order phase transition from *P2/n* to *C2/c*. As it was mentioned before, in the *P2/n* structure there are 4 M sites (two M1 and two M2) while in the *C2/c* structure, there are only 2 M sites. On the other hand, the analyzed omphacite formed at temperatures below 800°C, exhibits a cation ordering better described in space group *P2/c*, in which there are also 4 M sites, two M1 and two M2. This space group has been suggested by several authors (e.g., Matsumoto et al., 1975; Fleet et al., 1978; Carpenter, 1981; Putnis, 1992). However, to our knowledge, this is the first detailed report of the structure of omphacite in space group *P2/c*.

As it was mentioned previously, the formation of the garnet + omphacite assemblage, which is typical of the eclogitic stage, depends on the Ca/Na ratio and the total Na_2O content. The Ca/Na ratio becomes smaller as the pressure on the system increases stabilizing the albite phase. The stage of symplectite formation occurs upon decompression and cooling from eclogitic conditions in the presence of an aqueous fluid (e.g., Faryad et al., 2006; Ríos et al., 2017; Shuguang and Yi, 2021). The corresponding symplectites are characterized by the replacement of high pressure minerals by very fine-grained hydrated phases, where omphacite is rimmed by colonies of symplectites mainly composed of Na-rich plagioclase, Na-poor omphacite and Mg-hornblende, with minor amounts of edenite or pargasite. Omphacite grains (**Figures 5E,F**) in retrograded eclogites of the Arquía Complex are rimmed by symplectites that are successively composed of coarse-grained inner zone (first stage of formation), surrounded by a medium-grained texture

(intermediate stage of formation), and a fine-grained texture in the outermost zone (last stage of formation). We highlight that towards the coarse-grained symplectite the Ca content increases, and the Na content decreases, possibly due to a longer period of development, decompression and hydration from the omphacite. A textural variation of the symplectite colonies can be associated to the growth and generation of amphibole and plagioclase upon hydration and decompression. These results are consistent with symplectites that represent decompressed omphacite in relict eclogites (e.g., Peacock and Goodge, 1995; Zhao et al., 2001), and which would result from a rapid uplift and significant over-stepping of a strongly pressure dependent reaction along a nearly isothermal decompression path as suggested by Anderson and Moecher (2007). The isochemical nature of the symplectite-forming reaction is also commonly accepted (e.g., Shervais et al., 2003), and reintegrated symplectite assemblages are used to estimate an original omphacite composition. Uncertainties exist with the inferred exsolution mechanism and the isochemical assumption of symplectite formation (Anderson and Moecher, 2007).

In summary, omphacite decomposes into symplectites consisting of plagioclase + low Na clinopyroxene, a product of decompression and hydration through the reaction: omphacite + quartz = plagioclase + clinopyroxene (low in Na) (e.g., Elvevold and Gilotti, 2000; Mposkos et al., 2012), which can be considered a discontinuous precipitation reaction (Joanny et al., 1991). When the transformation to symplectite involves clinozoisite, the reaction is omphacite + clinozoisite + H_2O = amphibole + plagioclase (albite).

CONCLUSION

We report for the first time chemical and structural data on omphacite from the Arquía Complex on southwestern Pijao, Central Cordillera of the Colombian Andes. The analyzed omphacite crystallized in space group *P2/c*, one of the possible space groups in which this mineral may crystallize. The crystallization of omphacite in the *P2/c* space group may be interpreted as an intermediate stage towards the formation of equilibrium omphacite with space group *P2/n*. The structure of omphacite shows the Na and Ca cations at the 6 and 8 coordination sites. Fe occurs as Fe^{2+} and Fe^{3+} and is distributed over the octahedral M1 and M11 sites, respectively. All Fe^{3+} replace Al^{3+}, and Fe^{2+} replaces Mg at the M1 sites. Na and Ca are distributed on alternating M2 sites (M2 and M21). The structure is made of silicate chains formed by two crystallographically different silicon tetrahedra (T1 and T2) with an O2-O3-O2 angle of 169.002 (2)°, indicating that the chain is slightly distorted. The transformation of omphacite to symplectites colonies characterizes the initiation of the eclogites retrograde metamorphism.

DATA AVAILABILITY STATEMENT

The original contributions presented in the study are included in the article/Supplementary Material, further inquiries can be directed to the corresponding author.

AUTHOR CONTRIBUTIONS

All authors listed have made a substantial, direct, and intellectual contribution to the work and approved it for publication.

FUNDING

This research project was funded by the Microscopy and X-ray Laboratories of Vicerrectoría de Investigación y Extensión of Universidad Industrial de Santander and the Microscopy Laboratory of the Department of Geosciences of Universidad Nacional de Colombia.

ACKNOWLEDGMENTS

The authors gratefully acknowledge the Microscopy and X-ray Laboratories of Vicerrectoría de Investigación y Extensión of Universidad Industrial de Santander and the Microscopy Laboratory of the Department of Geosciences of Universidad Nacional de Colombia, and their professional staff for assistance with data acquisition. This study has benefited from these entities and their human resources. We express thanks to reviewers for helpful comments and suggestions of this manuscript. We are most grateful to the above-named people and institutions for support.

REFERENCES

Anderson, E. D., and Moecher, D. P. (2007). Omphacite Breakdown Reactions and Relation to Eclogite Exhumation Rates. *Contrib. Mineral. Petrol.* 154 (3), 253–277. doi:10.1007/s00410-007-0192-x

Arlt, T., Angel, R. J., Miletich, R., Armbruster, T., and Peters, T. (1998). High-Pressure P21/c-C2/c Phase Transitions in Clinopyroxenes; Influence of Cation Size and Electronic Structure. *Am. Mineral.* 83, 1176–1181. doi:10.2138/am-1998-11-1205

Arrieta-Prieto, M., Zuluaga-Castrillón, C., Castellanos-Alarcón, O., and Ríos-Reyes, C. (2020). Metamorphic Evolution of Raspas Complex (Ecuador) and its Relation with a J-K belt of Melanges in NW of the South American Plate. *EGU Gen. Assembly*, EGU2020–12395. doi:10.5194/egusphere-egu2020-12395

Ashchepkov, I., Medvedev, N., Ivanov, A., Vladykin, N., Ntaflos, T., Downes, H., et al. (2019). Deep Mantle Roots of the Zarnitsa Kimberlite Pipe, Siberian Craton, Russia: Evidence for Multistage Polybaric Interaction with Mantle Melts. *J. Asian Earth Sci.* 266, 197–219. doi:10.1016/j.jseaes.2021.104756

Aulbach, S., and Arndt, N. T. (2019). Eclogites as Palaeodynamic Archives: Evidence for Warm (Not Hot) and Depleted (But Heterogeneous) Archaean Ambient Mantle. *Earth Planet. Sci. Lett.* 505, 162–172. doi:10.1016/j.epsl.2018.10.025

Bakirov, A. B., Tagiri, M., and Sakiev, K. S. (1998). Rocks of Ultrahigh-Pressure Metamorphic Facies in the Tien Shan. *Russ. Geol. Geophys.* 39, 1709–1721.

Bascou, J., Barruol, G., Vauchez, A., Mainprice, D., and Egydio-Silva, D. (2001). EBSD-Measured Lattice-Preferred Orientation and Seismic Properties of Eclogites. *Tectonophysics* 342, 61–80. doi:10.1016/S0040-1951(01)00156-1

Black, P. M. (1970). P2 Omphacite, Intermediate in Composition between Jadeite and Hedenbergite, from Metamorphosed Acid Volcanics, Bouehndep, New Caledonia. *Am. Mineral.* 55, 512–514.

Boffa Ballaran, T., Carpenter, M. A., Domeneghetti, M. C., and Tazzoli, V. (1998). Structural Mechanisms of Solid Solution and Cation Ordering in Augite-Jadeite Pyroxenes; I, A Macroscopic Perspective. *Am. Mineral.* 83, 419–433. doi:10.2138/am-1998-5-60110.2138/am-1998-5-602

Boland, J. N., and van Roermund, H. L. M. (1983). Mechanisms of Exsolution in Omphacites from High Temperature, Type B, Eclogites. *Phys. Chem. Minerals* 9, 30–37. doi:10.1007/BF00309467

Buatier, M., van Roermund, H. L. M., Drury, M. R., and Lardeaux, J. M. (1991). Deformation and Recrystallization Mechanisms in Naturally Deformed Omphacites from the Sesia-Lanzo Zone; Geophysical Consequences. *Tectonophysics* 195 (1), 11–27. doi:10.1016/0040-1951(91)90141-E

Bustamante, A., Juliani, C., Essene, E. J., Hall, C. M., and Hyppolito, T. (2012). Geochemical Constraints on Blueschist- and Amphibolite-Facies Rocks of the Central Cordillera of Colombia: the Andean Barragán Region. *Int. Geology. Rev.* 54 (9), 1013–1030. doi:10.1080/00206814.2011.594226

Bustamante, A., Juliani, C., Hall, C., and Essene, E. (2011). $^{40}Ar/^{39}Ar$ Ages from Blueschists of the Jambaló Region, Central Cordillera of Colombia: Implications on the Styles of Accretion in the Northern Andes. *Geol. Acta* 9 (3-4), 351–362. doi:10.1344/105.000001697

Cameron, M., and Papike, J. J. (1981). Structural and Chemical Variations in Pyroxenes. *Am. Mineral.* 66, 1–50.

Carpenter, J. R., and Macaulay, W. L. (1979). Relapsing Polychondritis. *Arthritis Rheum.* 22, 102–103. doi:10.1002/art.1780220125

Carpenter, M. A., Domeneghetti, M.-C., and Tazzoli, V. (1990). Application of Landau Theory to Cation Ordering in Omphacite I: Equilibrium Behaviour. *Eur. J. Mineral.* 2, 7–18. doi:10.1127/ejm/2/1/0007

Carpenter, M. A. (1978). Kinetic Control of Ordering and Exsolution in Omphacite. *Contr. Mineral. Petrol.* 67, 17–24. doi:10.1007/bf00371629

Carpenter, M. A. (1981). Omphacite Microstructures as Time-Temperature Indicators of Blueschist- and Eclogite-Facies Metamorphism. *Contr. Mineral. Petrol.* 78, 441–451. doi:10.1007/BF00375206

Castellanos, O. M. (2021). Caracterización del metamorfismo de alta presión para eclogitas y esquistos azules, emplazados dentro del Complejo Arquía, en el sector Pijao-Génova (Quindío), flanco oeste, cordillera Central, Colombia. PhD Thesis. Bogotá, D.C., Colombia: Universidad Nacional de Colombia.

Clark, J. R., and Papike, J. J. (1968). Crystal-Chemical Characterization of Omphacites. *Am. Mineral.* 53, 840–868.

Elvevold, S., and Gilotti, J. A. (2000). Pressureâ€"temperature Evolution of Retrogressed Kyanite Eclogites, Weinschenk Island, Northâ€"East Greenland Caledonides. *Lithos* 53, 127–147. doi:10.1016/S0024-4937(00)00014-1

Essene, E., and Fyfe, W. (1967). Omphacite in California Metamorphic Rocks. *Contrib. Mineral. Petrol.* 15, 1–23. doi:10.1007/BF01167213

Faryad, S. W., Perraki, M., and Vrána, S. (2006). P-T Evolution and Reaction Textures in Retrogressed Eclogites from Svetlik, the Moldanubian Zone (Czech Republic). *Mineralogy Petrol.* 88 (1), 297–319. doi:10.1007/s00710-006-0142-8

Feng, P., Wang, L., Brown, M., Johnson, T. E., Kylander-Clark, A., and Piccoli, P. M. (2021). Partial Melting of Ultrahigh-Pressure Eclogite by Omphacite-Breakdown Facilitates Exhumation of Deeply-Subducted Crust. *Earth Planet. Sci. Lett.* 554, 116664. doi:10.1016/j.epsl.2020.116664

Fleet, M. E., Herzberg, C. T., Bancroft, G. M., and Aldridge, L. P. (1978). Omphacite Studies; I, the *P2/n* → *C2/c* Transformation. *Am. Mineral.* 63, 1100–1106.

García, C. A., Ríos, C. A., Castellanos, O. M., and Mantilla, L. C. (2017). Petrology, Geochemistry and Geochronology of the Arquía Complex´s Metabasites at the Pijao-Génova Sector, central Cordillera, Colombian Andes. *Bol. Geol.* 39 (1), 105–126. doi:10.18273/revbol.v39n1-2017005

García-Casco, A., Blanco, I., Ruiz, E. C., Moreno, M., Toro, L., Gómez, A., et al. (2011a). "Thermobarometry of Amphibolites from the Arquía Complex (Central Colombia): Geodynamic Implications," in Memorias XIV Congreso Latinoamericano de Geología, Medellín, Agosto, 30 a septiembre 2 de 2011.

García-Casco, A., Proenza, J. A., and Iturralde-Vinent, M. A. (2011b). Subduction Zones of the Caribbean: the Sedimentary, Magmatic, Metamorphic and Ore-deposit Records. UNESCO/iugs Igcp Project 546 Subduction Zones of the Caribbean. *Geol. Acta* 9 (3-4), 217–224. doi:10.1344/105.000001745

Gaston, G., and Roermund van, H. (1995). Deformation-Induced Clinopyroxene Fabrics From Eclogite. *J. Struct. Geol.* 17, 1425–1443. doi:10.1016/0191-8141(95)00038-F

González, I. H. (1997). *Metagabros y Eclogitas asociadas en el area de Barragán, Departamento del Valle, Colombia*. Colombia: Geología Colombiana 22, 151–170. Available at: https://revistas.unal.edu.co/index.php/geocol/article/view/31453.

Grosse, E. (1926). *El Terciario Carbonífero de Antioquia en la parte Occidental de la Cordillera Central de Colombia, entre el río Arma y Sacaojal*. Berlín: Dietrich Reimer Ernst Vohsen Editores, 361p.

Hastie, A., Kerr, A., Pearce, J., and Mitchell, S. (2007). Classification of Altered Volcanic Island Arc Rocks Using Immobile Trace Elements: Development of the Th Co Discrimination Diagram. *J. Petrol.* 48, 2341–2357. doi:10.1093/petrology/egm062

Holland, T., and Powell, R. (2003). Activity?composition Relations for Phases in Petrological Calculations: An Asymmetric Multicomponent Formulation. *Geochim. Cosmochim. Acta* 145 (145), 492–501. doi:10.1007/s00410-003-0464-z

Joanny, V., Lardeaux, J. M., Trolliard, G., and Boudeulle, M. (1989). La transition omphacite → diopside + plagioclase des les eclogites du Rouergue (Massif Central Francais): un example de precipitation discontinue. *Compt. Rend. Hebd. Séances Acad. Sci.* 309 (2), 1923–1930.

Joanny, V., van Roermund, H., and Lardeaux, J. M. (1991). The Clinopyroxene/Plagioclase Symplectite in Retrograde Eclogites: A Potential Geothermobarometer. *Geol. Rundsch* 80 (2), 303–320. doi:10.1007/BF01829368

Kabir, M. F., and Takasu, A. (2010). Evidence for Multiple Burial-Partial Exhumation Cycles from the Onodani Eclogites in the Sambagawa Metamorphic Belt, Central Shikoku, Japan. *J. Metamorph. Geol.* 28 (8), 873–893. doi:10.1111/j.1525-1314.2010.00898.x

Katerinopoulou, A., Katerinopoulos, A., Bieniok, A., KnopMagganas, E. A., Magganas, A., and Amthauer, G. (2007). Crystal Chemistry, Structure Analyses and Phase Transition experiment on an Omphacite from Eclogitic Metagabbro from Syros Island, Greece. *Mineralogy Petrol.* 91, 117–128. doi:10.1007/s00710-007-0185-5

Li, J.-L., Klemd, R., Gao, J., and John, T. (2016). Poly-Cyclic Metamorphic Evolution of Eclogite: Evidence for Multistage Burial-Exhumation Cycling in a Subduction Channel. *J. Petrol.* 57 (1), 119–146. doi:10.1093/petrology/egw002

Liu, H., Zhang, K., Ingrin, J., and Yang, X. (2021). Electrical Conductivity of Omphacite and Garnet Indicates Limited Deep Water Recycling by Crust Subduction. *Earth Planet. Sci. Lett.* 559, 116784. doi:10.1016/j.epsl.2021.116784

Maresch, W. V., and Abraham, K. (1981). Petrography, Mineralogy, and Metamorphic Evolution of an Eclogite from the Island of Margarita, Venezuela. *J. Petrol.* 22 (3), 337–362. doi:10.1093/petrology/22.3.337

Martin, C., and Duchêne, S. (2015). Residual Water in Hydrous Minerals as a Kinetic Factor for Omphacite Destabilization into Symplectite in the Eclogites of Vårdalsneset (WGR, Norway). *Lithos* 232, 162–173. doi:10.1016/j.lithos.2015.06.021

Matsumoto, K., and Hirajima, T. (2005). The Coexistence of Jadeite and Omphacite in an Eclogite-Facies Metaquartz Diorite from the Southern Sesia Zone, Western Alps, Italy. *J. Mineralogical Petrological Sci.* 100, 70–84. doi:10.2465/jmps.100.70

Matsumoto, T., and Banno, S. (1970). A Natural Pyroxene with the Space Group C42h-P2/n. *Proc. Jpn. Acad.* 46, 173–175. doi:10.2183/pjab1945.46.173

Matsumoto, T., Tokonami, M., and Morimoto, N. (1975). The crystal Structure of Omphacite. *Am. Mineral.* 60, 634–641.

McCourt, W., and Feininger, T. (1984). High Pressure Metamorphic Rocks in the Central Cordillera of Colombia. *BGS Rep. Ser.* 85 (1), 28–35.

McCourt, W., Mosquera, D., Nivia, A., and Nuñez, A. (1984). Mapa geológico preliminar de la Plancha 243 - Armenia. Esc. 1:100.000, INGEOMINAS.

McNamara, D. D. (2012). Omphacite-a mineral under Pressure!. *Geol. Today* 28, 71–75. doi:10.1111/j.1365-2451.2012.00830.x

Meschede, M. (1986). A Method of Discriminating Between Different Types of Mid-Ocean Ridge Basalts and Continental Tholeiites with the Nb-Zr-Y Diagram. *Chem. Geol.* 56, 207–218. doi:10.1016/0009-2541(86)90004-5

Miyagi, Y., and Takasu, A. (2005). Prograde Eclogites from the Tonaru Epidote Amphibolite Mass in the Sambagawa Metamorphic Belt, central Shikoku, Southwest Japan. *Isl. Arc* 14, 215–235. doi:10.1111/j.1440-1738.2005.00468.x

Moghadam, R. H., Trepmann, C. A., Stöckhert, B., and Renner, J. (2010). Rheology of Synthetic Omphacite Aggregates at High Pressure and High Temperature. *J. Petrol.* 51, 921–945. doi:10.1093/petrology/egq006

Morimoto, N. (1988). Nomenclature of Pyroxenes. *Mineralogy and Petrology* 39, 55–76. doi:10.1007/BF01226262

Mosquera, D. (1978). *Geología del Cuadrángulo K-8 Manizales*. Inf. interno, INGEOMINAS, 1–78. Available at: https://catalogo.sgc.gov.co/cgi-bin/koha/opac-detail.pl?biblionumber=11225

Mottana, A., Murata, T., Wu, Z., Marcelli, A., and Paris, E. (1997). The Local Structure of Ca-Na Pyroxenes. I. XANES Study at the Na K-Edge. *Phys. Chem. Minerals* 24, 500–509. doi:10.1007/s002690050065

Moulas, E., Tajčmanová, L., Vrijmoed, J. C., and Podladchikov, Y. (2015). Mechanically- V . Diffusion-Controlled Metamorphic Microstructure: a Symplectite Example from Rhodope Metamorphic Complex (Greece). *J. Metamorph. Geol.* 33 (8), 849–858. doi:10.1111/jmg.12141

Mposkos, E., Baziotis, I., and Proyer, A. (2012). Pressure-Temperature Evolution of Eclogites from the Kechros Complex in the Eastern Rhodope (NE Greece). *Int. J. Earth Sci. (Geol Rundsch)* 101 (4), 973–996. doi:10.1007/s00531-011-0699-2

Murcia, A., and Cepeda, H. (1991a). Mapa geológico de la Plancha 410 – La Unión. Escala 1:100.000. INGEOMINAS.

Murcia, A., and Cepeda, H. (1991b). Mapa geológico de la Plancha 429 – Pasto. Escala 1:100.000. INGEOMINAS.

Mysen, B. O., and Griffin, W. L. (1973). Pyroxene Stoichiometry and the Breakdown of Omphacite. *Am. Mineral.* 58, 60–63.

Nakamura, D., and Banno, S. (1997). Thermodynamic Modelling of Sodic Pyroxene Solid-Solution and its Application in a Garnet-Omphacite-Kyanite-Coesite Geothermobarometer for UHP Metamorphic Rocks. *Contrib. Mineralogy Petrol.* 130, 93–102. doi:10.1007/s004100050352

Nakano, N., Osanai, Y., Sajeev, K., Hayasaka, Y., Miyamoto, T., Minh, N. T., et al. (2010). Triassic Eclogite from Northern Vietnam: Inferences and Geological Significance. *J. Metamorph. Geol.* 28, 59–76. doi:10.1111/j.1525-1314.2009.00853.x

Orrego, A., Cepeda, H., and Rodríguez, G. (1980a). Esquistos glaucofánicos en el área de Jambaló, Cauca (Colombia). *Nota Preliminar. Geol. Norand.* 1, 5–10.

Orrego, A., Restrepo, J., Toussaint, J., and Linares, E. (1980b). Datación de un esquisto sericítico de Jambaló - Cauca. *Pub. Esp. Geol. Univ. Nal.* 25, 133–134.

Pandolfo, F., Nestola, F., Camara, F., and Domeneghetti, M. C. (2012). High-pressure Behavior of Space Group *P2/n* Omphacite. *Am. Mineral.* 97 (2-3), 407–414. doi:10.2138/am.2012.3928

Pavese, A., Bocchio, R., and Ivaldi, G. (2000). *In Situ* high Temperature Single crystal X-ray Diffraction Study of a Natural Omphacite. *Mineral. Mag.* 64, 983–993. doi:10.1180/002646100549986

Peacock, S. M., and Goodge, J. W. (1995). Eclogite-facies Metamorphism Preserved in Tectonic Blocks from a Lower Crustal Shear Zone, central Transantarctic Mountains, Antarctica. *Lithos* 36, 1–13. doi:10.1016/0024-4937(95)00006-2

Pearce, J. (1982). Trace Element Characteristics of Lavas from Destructive Plate Boundaries In *book: Andesites: Orogenic Andesites and Related Rocks*. Editors R. S. Thorpe (John Wiley and Sons), 525–548.

Pearce, J. (2008). Geochemical Fingerprinting of Oceanic Basalts With Applications to Ophiolite Classification and the Search for Archean Oceanic Crust. *Lithos* 100, 14–48. doi:10.1016/j.lithos.2007.06.016

Putnis, A. (1992). *Introduction to Mineral Sciences*. Cambridge, UK: Cambridge University Press, 457p.

Råheim, A., and Green, D. H. (1974). Experimental Determination of the Temperature and Pressure Dependence of the Fe-Mg Partition Coefficient for Coexisting Garnet and Clinopyroxene. *Contr. Mineral. Petrol.* 48, 179–203. doi:10.1007/BF00383355

Restrepo, J., and Toussaint, J. (1974). *Algunas consideraciones sobre la evolución estructural de los Andes Colombianos*. Medellín: Pub. Esp. Geol., Departamento de Ciencias de la Tierra, Facultad de Ciencias, Universidad Nacional de Colombia, 4, 1–14.

Rigaku (2015b). *CrysAlisPro Software System*, 171.39.28e. Oxford, UK: Rigaku Corporation.

Rigaku (2015a). "CrystalClear-SM Expert, 2.1 B45," in *Rigaku: Rigaku Americas* (The Woodlands, TX, USA, Tokyo, Japan: Rigaku Corporation).

Ríos, C. A., Castellanos, O. M., Ríos, V., and y Gómez, C. (2008). Una contribución al estudio de la evolución tectono-metamórfica de las rocas de alta-P, Cordillera Central, Andes Colombianos. *Geol. Colomb.* 33, 3–22.

Ríos, C. A., Castellanos-Alarcón, O. M., and García-Ramírez, C. A. (2017). Petrogenetic Significance of the Eclogites from the Arquía Complex on Southwestern Pijao, Central Cordillera (Colombia Andes). *DYNA* 84 (200), 291–301. doi:10.15446/dyna.v84n200.48166

Robinson, K., Gibbs, G. V., and Ribbe, P. H. (1971). Quadratic Elongation: A Quantitative Measure of Distortion in Coordination Polyhedra. *Science* 172 (3983), 567–570. doi:10.1126/science.172.3983.567

Ross, N. L., and Reynard, B. (1999). The Effect of Iron on the P21lc to C2/c Transition in (Mg,Fe)SiO3 Clinopyroxenes. *Eur. J. Mineral.* 11, 585–590. doi:10.1127/ejm/11/3/0585

Rossi, G., Smith, D. C., Ungaretti, L., and Domeneghetti, M. C. (1983). Crystal-chemistry and Cation Ordering in the System Diopside-Jadeite: a Detailed Study by crystal Structure Refinement. *Contr. Mineral. Petrol.* 83, 247–258. doi:10.1007/BF00371193

Ruiz, E. C., Blanco, I. F., Toro, L. M., Moreno, M., Vinasco, C. J., García-Casco, A., et al. (2012). Geoquímica y petrología de las metabasitas del Complejo Arquía (Municipio de Santafé de Antioquia y Río Arquía, Colombia): Implicaciones geodinámicas. *Bol. Cie. Tierra* 32, 65–80.

Sasaki, S., Matsumoto, T., and Sawada, C. (1981). The Influence of Multiple Diffraction on the Space Group Determination of Orthopyroxene, Spodumene, Low Omphacite and Pigeonite. *Phys. Chem. Minerals.* 7, 260–267. doi:10.1007/bf00311978

Schorn, S., Hartnady, M. I. H., Diener, J. F. A., Clark, C., and Harris, C. (2021). H2O-fluxed Melting of Eclogite during Exhumation: an Example from the Eclogite Type-Locality, Eastern Alps (Austria). *Lithos* 390-391, 106118. doi:10.1016/j.lithos.2021.106118

Sheldrick, G. M. (2015b). Crystal Structure Refinement withSHELXL. *Acta Crystallogr. C* 71 (1), 3–8. doi:10.1107/S2053229614024218 3

Sheldrick, G. M. (2015a). SHELXT- Integrated Space-Group and crystal-structure Determination. *Acta Cryst. Sect A.* 71 (1), 3–8. doi:10.1107/S2053273314026370

Sheng, Y.-M., and Gong, B. (2017). Hydrous Species in Eclogitic Omphacite: Implication for Metamorphic Dehydration during Exhumation. *J. Asian Earth Sci.* 145, 123–129. doi:10.1016/j.jseaes.2016.12.020

Shervais, J. W., Dennis, A. J., McGee, J. J., and Secor, D. (2003). Deep in the Heart of Dixie: Pre-Alleghanian Eclogite and HP Granulite Metamorphism in the Carolina Terrane, South Carolina, USA. *J. Metamorph. Geol.* 21, 65–80. doi:10.1046/j.1525-1314.2003.00416.x

Shu, Q., Brey, G. P., Gerdes, A., and Hoefer, H. E. (2014). Mantle Eclogites and Garnet Pyroxenites - the Meaning of Two-point Isochrons, Sm-Nd and Lu-Hf Closure Temperatures and the Cooling of the Subcratonic Mantle. *Earth Planet. Sci. Lett.* 389, 143–154. doi:10.1016/j.epsl.2013.12.028

Sizova, E., Gerya, T., Brown, M., and Perchuk, L. L. (2010). Subduction Styles in the Precambrian: Insight from Numerical Experiments. *Lithos* 116, 209–229. doi:10.1016/j.lithos.2009.05.028

Skelton, R., and Walker, A. M. (2015). The Effect of Cation Order on the Elasticity of Omphacite from Atomistic Calculations. *Phys. Chem. Minerals* 42 (8), 677–691. doi:10.1007/s00269-015-0754-9

Smith, D. C., Mottana, A., and Rossi, G. (1980). Crystal-chemistry of a Unique Jadeite-Rich Acmite-Poor Omphacite from the Nybø Eclogite Pod, Sørpollen, Nordfjord, Norway. *Lithos* 13, 227–236. doi:10.1016/0024-4937(80)90068-7

Song, S., and Cao, Y. (2021). "Textures and Structures of Metamorphic Rocks," in *Encyclopedia of Geology*. Editors D. Alderton and E. A. Scott. 2nd edition (United Kingdom: Academic Press), 2, 375–388. doi:10.1016/B978-0-08-102908-4.00052-7

Su, W., Zhang, M., Chen, J., Bromiley, G. D., Ye, K., Redfern, S. A. T., et al. (2011). Amorphization in Natural Omphacite and its Implications. *J. Asian Earth Sci.* 42 (4), 694–703. doi:10.1016/j.jseaes.2010.10.001

Tsujimori, T., and Liou, J. G. (2004). Coexisting Chromian Omphacite and Diopside in Tremolite Schist from the Chugoku Mountains, SW Japan: The Effect of Cr on the Omphacite-Diopside Immiscibility gap. *Am. Mineral.* 89, 7–14. doi:10.2138/am-2004-0102

Tsujimori, T., Liou, J. G., and Coleman, R. G. (2005). Coexisting Retrograde Jadeite and Omphacite in a Jadeite-Bearing Lawsonite Eclogite from the Motagua Fault Zone, Guatemala. *Am. Mineral.* 90, 836–842. doi:10.2138/am.2005.1699

Ulrich, S., and Mainprice, D. (2005). Does Cation Ordering in Omphacite Influence Development of Lattice-Preferred Orientation? *J. Struct. Geology.* 27 (3), 419–431. doi:10.1016/j.jsg.2004.11.003

van Hunen, J., and Moyen, J.-F. (2012). Archean Subduction: Fact or Fiction? *Annu. Rev. Earth Planet. Sci.* 40, 195–219. doi:10.1146/annurev-earth-042711-105255

Villagómez, D., Spikings, R., Magna, T., Kammer, A., Winkler, W., and Beltran, A. (2011). Geochronology, Geochemistry and Tectonic Evolution of the Western and Central Cordilleras of Colombia. *Lithos* 125, 875–896. doi:10.1016/j.lithos.2011.05.003

Vinograd, V. L., Gale, J. D., and Winkler, B. (2007). Thermodynamics of Mixing in Diopside-Jadeite, CaMgSi2O6-NaAlSi2O6, Solid Solution from Static Lattice Energy Calculations. *Phys. Chem. Minerals* 34, 713–725. doi:10.1007/s00269-007-0189-z

Wang, J.-M., Lanari, P., Wu, F.-Y., Zhang, J.-J., Khanal, G. P., and Yang, L. (2021). First Evidence of Eclogites Overprinted by Ultrahigh Temperature Metamorphism in Everest East, Himalaya: Implications for Collisional Tectonics on Early Earth. *Earth Planet. Sci. Lett.* 558, 116760. doi:10.1016/j.epsl.2021.116760

Whitney, D. L., and Evans, B. W. (2010). Abbreviations for Names of Rock-Forming Minerals. *Am. Mineral.* 95, 185–187. doi:10.2138/am.2010.3371

Xie, Z., Liu, X., Jin, Z., and Li, Z. (2020). Microstructures and Phase Transition in Omphacite: Constraints on the P-T Path of Shuanghe Eclogite (Dabie Orogen). *J. Earth Sci.* 31, 254–261. doi:10.1007/s12583-019-1279-9

Yokoyama, K., and Sameshima, T. (1982). Miscibility gap between Jadeite and Omphacite. *Mineralogical J.* 11, 53–61. doi:10.2465/minerj.11.53

Zhang, D., Hu, Y., and Dera, P. K. (2016). Compressional Behavior of Omphacite to 47 GPa. *Phys. Chem. Minerals* 43, 707–715. doi:10.1007/s00269-016-0827-4

Zhang, J., Green, H. W., II, and Bozhilov, K. N. (2006). Rheology of Omphacite at High Temperature and Pressure and Significance of its Lattice Preferred Orientations. *Earth Planet. Sci. Lett.* 246 (3-4), 432–443. doi:10.1016/j.epsl.2006.04.006

Zhang, J., and Green, H. W., II (2007). Experimental Investigation of Eclogite Rheology and its Fabrics at High Temperature and Pressure. *J. Metamorph. Geol.* 25 (2), 97–115. doi:10.1111/j.1525-1314.2006.00684.x

Zhang, Q., Ma, Z., and Shi, N. (1999). Determination of crystal Structure of Omphacite. *Chin. Sci. Bull.* 44, 944–949. doi:10.1007/bf02885072

Zhang, Y. (1998). Mechanical and Phase Equilibria in Inclusion-Host Systems. *Earth Planet. Sci. Lett.* 157, 209–222. doi:10.1016/S0012-821X(98)00036-3

Zhao, G., Cawood, P. A., Wilde, S. A., and Lu, L. (2001). High-pressure Granulites (Retrograded Eclogites) from the Hengshan Complex, North China Craton: Petrology and Tectonic Implications. *J. Petrol.* 42, 1141–1170. doi:10.1093/petrology/42.6.1141

Conflict of Interest: The authors declare that the research was conducted in the absence of any commercial or financial relationships that could be construed as a potential conflict of interest.

Publisher's Note: All claims expressed in this article are solely those of the authors and do not necessarily represent those of their affiliated organizations, or those of the publisher, the editors and the reviewers. Any product that may be evaluated in this article, or claim that may be made by its manufacturer, is not guaranteed or endorsed by the publisher.